ACADEMIC PRESS

Available online at www.sciencedirect.com

SCIENCE DIRECT®

Journal of Computational Physics 186 (2003) 93–121

JOURNAL OF COMPUTATIONAL PHYSICS

www.elsevier.com/locate/jcp

Time-dependent algorithms for the simulation of viscoelastic flows with spectral element methods: applications and stability

Nicolas Fiétier, Michel O. Deville *

Laboratory of Computational Engineering, School of Engineering, Ecole Polytechnique Fédérale de Lausanne, CH-1015 Lausanne, Switzerland

Received 4 April 2001; received in revised form 11 February 2002; accepted 21 December 2002

Abstract

This paper presents the development of spectral element methods to simulate unsteady flows of viscoelastic fluids using a closed-form differential constitutive equation. The generation and decay Poiseuille planar flows are considered as benchmark problems to test the abilities of our computational method to deal with truly time-dependent flows. Satisfactory results converging toward steady-state regimes have been obtained for the flow through a four-to-one planar abrupt contraction with unsteady algorithms. Time-dependent simulations of viscoelastic flows are prone to numerical instabilities even for simple geometrical configurations. Possible methods to improve the numerical stability of the computational algorithms are discussed in view of the results carried out with numerical simulations for the flows through a straight channel and the four-to-one contraction.

Keywords: Spectral elements; Viscoelastic fluids; Transient algorithms; Computational stability

1. Introduction

Non-Newtonian fluids present many effects that cannot be predicted by classical viscous fluid mechanics. Among them, viscoelastic fluids are characterized by specific features like the shear-rate dependence of the shear viscosity, the presence of normal stresses in viscometric flows, the high resistance to elongational deformations and the memory effects related to their elastic properties. In parallel to the experimental investigations, various models have been used in computer programs in order to simulate the behavior of non-Newtonian fluids. Relatively simple models like the upper-convected Maxwell (UCM) and Oldroyd-B equations have been introduced first in viscoelastic flow simulations. Even though they contain both viscous and elastic properties suitable for benchmark problems, their restricted adequacy when simulations

* Corresponding author. Tel.: +41-21-693-5318; fax: +41-21-693-3646.
E-mail address: michel.deville@epfl.ch (M.O. Deville).

0021-9991/03/$ - see front matter
doi:10.1016/S0021-9991(03)00013-5

are compared to experiments induced the development and use of many other constitutive relationships like for instance the FENE dumbbell [4] or Phan-Thien–Tanner (PTT) [38] models, derived from the kinetic and network theory, which present the desirable features of shear-thinning and finite elongational viscosity. However, it must be stressed that none of the existing models can generate realistic predictions for all type of deformations of any given fluid. Other more sophisticated models like the so-called "Pom-Pom" model [32] fitted to the behavior of specific types of polymers have been proposed but their use is restricted to special cases.

The mathematical model of viscoelastic flows consists of the set of three-coupled equations which are to be solved simultaneously, namely the continuity and momentum equations (which are related to the conservation of mass and momentum) in addition to the constitutive equation (in which viscous and elastic characteristics of the fluid appear). The last equation has a tremendous impact on the results of numerical simulations and on the stability of the method. Both differential and integral constitutive models have been proposed. The Lagrangian formulation is used when dealing with integral models. Such flow computation implies solving a transient problem from given initial particle positions and a given deformation history. The domain of integration is then a time-dependent material volume, which renders the problem treatment rather difficult. Another emerging alternative to deal with time-dependent flows is to use a kinetic theory model (microscopic formulation) for evaluating the extra-stress, which results in decoupling the Eulerian solution of the conservation equations (computed by solving partial differential equations) from the computation of the extra-stress obtained by solving along particle paths a stochastic differential equation, e.g. [7,44]. Beyond their apparent complexity, the advantage of the "non-differential" models is that the associated computational methods are less prone to unstable behavior of the solution. However, in this paper, we will restrict ourselves to differential constitutive equations.

There is a growing interest in developing numerical tools to investigate the onset of instabilities observed in experiments involving viscoelastic flows [28], which is a difficult and challenging task as the simulations are very sensitive to numerical instabilities [43]. In the future, we will try to use the spectral element method to resolve such a physical instability in a benchmark problem. Most simulations involving viscoelastic fluids have been carried out for steady flows. As far as the spatial discretization is concerned, the most popular methods have been by far based on finite volumes and finite elements. Recently, alternate techniques based on Legendre spectral element methods have been applied with success to simulate steady viscoelastic flows, e.g. [10,35,48]. They combine the ability to treat complicated geometries like the classical (low-order) finite element methods with the accuracy of high-order approximation polynomials encountered in spectral methods. An example of complex viscoelastic flow computation is given for the two-dimensional four-to-one planar abrupt contraction benchmark problem. Simulations of unsteady flows are made more complicated by the presence of numerical instabilities due to the introduction of time in the equations in addition to the spatial ones related to the domain discretization that also exist with steady solvers [19,20]. Since numerical instabilities appear even in simple benchmark problems like the Couette [8,27] and Poiseuille flows of UCM and Oldroyd-B fluids, which have been shown to be stable [40,45,51] at zero Reynolds number, we have tested computational algorithms on these types of problems for which analytical solutions are available.

We resort for the time integration scheme to well-proven splitting techniques that have been applied to the transient Navier–Stokes equations. Some specific developments are introduced to handle the additional terms and equations brought by the non-Newtonian model. The C++ toolbox Speculoos [17] has been used and adapted to handle viscoelastic flow problems for the various simulations described in this paper.

In this paper, we investigate the sources of numerical instabilities occuring in the simulation of time-dependent flows of viscoelastic fluids by direct numerical simulations. A complementary approach based on linear stability analyses has been also used to study the effects of both spatial and temporal discretizations on the stability [22]. Additional examples of simulations of two-dimensional and three-dimensional flows of viscoelastic fluids may be found in [21].

The paper is organized as follows. The conservation equations and rheological models restricted to the FENE type (UCM, Oldroyd-B, FENE-CR, FENE-P) that we have considered are introduced in Sections 2.1 and 2.2. The spectral element method and relevant stabilization techniques are presented in Sections 3.1, 3.2 and 3.3. Computational algorithms are described in Sections 4.1 and 4.2 and referred to in Section 4.3. In addition to the simple Poiseuille viscoelastic flows in Section 5.1 for which analytical or numerical solutions can be easily determined, the more complicated reference problem of the flow through an abrupt planar four-to-one contraction is presented in Section 5.2. Results of computations for both type of flows are discussed in Sections 6.1, 6.2 and 6.3.

2. Governing equations

In this section, we present the basic continuous conservation equations in addition to the FENE constitutive relations and their simplified versions (UCM and Oldroyd-B), in a non-dimensional form. The velocity $\mathbf{v}$, coordinates $\mathbf{x}$, viscoelastic stress $\boldsymbol{\tau}$, pressure p and time t are, respectively, scaled with the following quantities: V (reference velocity), L_r (reference length), $S = \mu_t V/L_r$, $P = S$, $T = \rho L_r^2/\mu_t$, where ρ and μ_t are the fluid density and (total) viscosity.

2.1. Conservation equations

The continuity equation for incompressible fluids enforces a divergence-free velocity field. The momentum equation is modified with respect to the Newtonian case in order to account for the additional contribution due to the extra-stress tensor. The set of conservation equations reads:

$$\nabla \cdot \mathbf{v} = 0, \tag{1}$$

$$\frac{\partial \mathbf{v}}{\partial t} = -Re(\mathbf{v} \cdot \nabla)\mathbf{v} - \nabla p + R_\mu \nabla^2 \mathbf{v} + \nabla \cdot \boldsymbol{\tau} \tag{2}$$

with

$$\boldsymbol{\tau} = \boldsymbol{\sigma} + p\mathbf{I} - 2R_\mu \mathbf{D}. \tag{3}$$

The symbols $\boldsymbol{\sigma}$, $\mathbf{I}$ and $\mathbf{D}$ are, respectively, the Cauchy stress, identity and rate-of-deformation tensors. The latter is defined by

$$\mathbf{D} = \frac{1}{2}(\nabla \mathbf{v} + (\nabla \mathbf{v})^{\mathrm{T}}). \tag{4}$$

The pressure scalar field enforces the continuity constraint imposed by Eq. (1). The extra-stress tensor is split into two parts, namely a Newtonian one $2R_\mu \mathbf{D}$ and a viscoelastic one $\boldsymbol{\tau}$. The parameters R_μ and Re are the ratio of (Newtonian) solvent to total viscosities (μ_N/μ_t) and the Reynolds number ($\rho V L_r/\mu_t$). In Eq. (4), $(\nabla \mathbf{v})^{\mathrm{T}}$ is the transpose of $\nabla \mathbf{v}$, the velocity gradient.

2.2. Differential constitutive models

We have considered particular models of the FENE-dumbbell type. It is then customary to introduce a non-dimensional configuration tensor $\mathbf{A}$, which is related to the viscoelastic contribution $\boldsymbol{\tau}$ of the extra-stress tensor. As opposed to other models, the constitutive equation is separated into two parts: an evolution equation for the dumbbells and an expression for the polymer stress in order to produce a clear representation

of the polymer microstructure and of its dynamic influence. The FENE-CR model [12] has been introduced to obtain an equation as simple as possible while including the constant shear viscosity characteristics of a Boger fluid and allowing only finite extensibility of the dumbbells. The FENE-P model [4] is a close version, which enables to take into account shear-thinning effects present in many viscoelastic fluids.

For both FENE models, the relation between the viscoelastic stress and configuration tensors is given by:

$$\boldsymbol{\tau} = \frac{1 - R_\mu}{We} \frac{1}{1 - (\mathrm{tr}(\mathbf{A})/L_e^2)} (\mathbf{A} - f(\mathrm{tr}(\mathbf{A}))\mathbf{I}). \tag{5}$$

The configuration tensor $\mathbf{A}$ satisfies the following differential equation:

$$\left(1 - \frac{\mathrm{tr}(\mathbf{A})}{L_e^2}\right)\left(E\frac{\partial \mathbf{A}}{\partial t} + We((\mathbf{v}\cdot\nabla)\mathbf{A} - \mathbf{A}\cdot(\nabla\mathbf{v})^{\mathrm{T}} - \nabla\mathbf{v}\cdot\mathbf{A})\right) + \mathbf{A} = f(\mathrm{tr}(\mathbf{A}))\mathbf{I} \tag{6}$$

with

$$f(\mathrm{tr}(\mathbf{A})) = \frac{1 - (\mathrm{tr}(\mathbf{A})/L_e^2)}{K} \quad \text{(FENE-P)} \tag{7}$$

or

$$f(\mathrm{tr}(\mathbf{A})) = 1 \quad \text{(FENE-CR)}. \tag{8}$$

In Eq. (5), $1 - R_\mu$ is the non-dimensional viscosity ($1 - R_\mu = \mu_P/\mu_t$ with $\mu_P = \mu_t - \mu_N$) of the polymeric component of the fluid. The symbol tr denotes the trace.

In Eq. (7), K is usually taken as: $K = 1 - (3/L_e^2)$. The parameter L_e measures the extensibility of the dumbbells. In some papers, K is equal to 1. When $L_e \to \infty$, the FENE-P and FENE-CR models are equivalent to the Oldroyd-B model. The upper-convected Maxwell (UCM) model corresponds to an Oldroyd-B model where $R_\mu = 0$.

The parameters $We = \lambda(V/L_r)$ and $E = We/Re = (\lambda\mu_t)/(\rho L_r^2)$ are, respectively, the Weissenberg and elastic number based on the relaxation time λ, density ρ, total dynamic viscosity μ_t, reference velocity V and length L_r. They are somehow indicators of elastic effects in the flow.

It must be emphasized that the presence of E in Eq. (6) is due to the particular scaling used for time $(\rho L_r^2/\mu_t)$ related to viscous effects as indicated in Section 1. As Re is decreased and goes to 0, the factor in front of the partial derivative with respect to time becomes infinite. In order for the whole term $E(\partial\mathbf{A}/\partial t)$ to remain finite, the partial derivative must vanish, which means that the configuration and viscoelastic stresses remain constant with respect to time so that no memory-induced effects (typical of viscoelastic fluids) are present and the fluid tends to behave as Newtonian. If the inertial time L_r/V would have been used for non-dimensionalization, E should be replaced by We in the factor of the time partial derivative. Both types of scaling have been used in the literature depending on the kind of flows (inertia or viscosity-dominated) to be investigated.

3. Spectral element formulation

In this section, we will first present the spectral element method based on the Galerkin formulation. Since we need a high-order method which is not numerically dissipative and dispersive in order to avoid erroneous simulation of the physics involved in the stress boundary layers, a spectral element method using Legendre polynomials is considered as a good candidate for discretizing the non-linear set of partial differential equations that model the flow.

3.1. Basic formulation

The problem consisting of solving the continuity, momentum and constitutive equations (1)–(6) on a flow domain $\Omega \subset \mathbb{R}^d$, where d is the problem dimension, in order to determine the three variables (pressure, velocity and viscoelastic stress) can be expressed with a general weak (Galerkin) formulation, which is also used in the finite element context.

To this end, it is necessary to define first a set of functional spaces X_p, X_v and X_τ to which the functions representing, respectively, the pressure p, velocity $\mathbf{v}$ and viscoelastic stress $\boldsymbol{\tau}$ will belong. These spaces are, respectively, subspaces of $L^2(\Omega)$, $H^1(\Omega)^d$ and $L^2(\Omega)^{d\times d}$, where $L^2(\Omega)$ and $H^1(\Omega)$ represent the space of measurable functions that are square-integrable on Ω and the space of derivable functions of which first order partial derivatives are measurable and square-integrable on Ω. Their definitions include the specification of boundary conditions.

Second, multilinear forms A, B and C involving the three variables can be defined based on integral inner products with test functions belonging to the functional spaces. The initial problem is then expressed in the weak formulation as:

Find $(p, \mathbf{v}, \boldsymbol{\tau}) \in X_p \times X_v \times X_\tau$ such that:

$$A(\mathbf{v}, \Psi_p) = \int_\Omega (\nabla \cdot \mathbf{v}) \Psi_p \, \mathrm{d}\Omega = 0 \quad \forall \Psi_p \in X_p \subset L^2(\Omega), \tag{9}$$

$$\begin{aligned} B(p, \mathbf{v}, \boldsymbol{\tau}, \Psi_v) = {} & \int_\Omega \frac{\partial \mathbf{v}}{\partial t} \cdot \Psi_v \, \mathrm{d}\Omega + \int_\Omega -p(\mathbf{I} : \nabla \Psi_v) \, \mathrm{d}\Omega \\ & + R_\mu \int_\Omega (\nabla \mathbf{v}) : \nabla \Psi_v \, \mathrm{d}\Omega + Re \int_\Omega [(\mathbf{v} \cdot \nabla)\mathbf{v}] \cdot \Psi_v \, \mathrm{d}\Omega + \int_\Omega \boldsymbol{\tau} \cdot \nabla \Psi_v \, \mathrm{d}\Omega \\ & - \int_{\partial\Omega} (\boldsymbol{\sigma} \cdot \mathbf{n}) \cdot \Psi_v \, \mathrm{d}\Gamma = 0 \quad \forall \Psi_v \in X_v \subset H^1(\Omega)^d, \end{aligned} \tag{10}$$

where the tensor product : is defined for two arbitrary tensors $\mathbf{P}$ and $\mathbf{Q}$ by:

$$\mathbf{P} : \mathbf{Q} = \mathbf{P}_{ij}\mathbf{Q}_{ij}, \quad 1 \leqslant i, j \leqslant d \tag{11}$$

using the usual convention of summation over repeated indices. The FENE-P or FENE-CR constitutive equation in weak form reads:

$$\begin{aligned} C(\mathbf{v}, \mathbf{A}, \Psi_A) = {} & \frac{We}{Re} \int_\Omega \left(1 - \frac{\mathrm{tr}(\mathbf{A})}{L_e^2}\right) \frac{\partial \mathbf{A}}{\partial t} : \Psi_A \, \mathrm{d}\Omega + We \int_\Omega \mathbf{A} : \Psi_A \, \mathrm{d}\Omega \\ & + We \int_\Omega \left(1 - \frac{\mathrm{tr}(\mathbf{A})}{L_e^2}\right) ((\mathbf{v} \cdot \nabla)\mathbf{A}) : \Psi_A \, \mathrm{d}\Omega - We \int_\Omega \left(1 - \frac{\mathrm{tr}(\mathbf{A})}{L_e^2}\right) (\nabla \mathbf{v} \cdot \mathbf{A}) : \Psi_A \, \mathrm{d}\Omega \\ & - We \int_\Omega \left(1 - \frac{\mathrm{tr}(\mathbf{A})}{L_e^2}\right) (\mathbf{A} \cdot (\nabla \mathbf{v})^{\mathrm{T}}) : \Psi_A \, \mathrm{d}\Omega - \int_\Omega f(\mathrm{tr}(\mathbf{A})\mathbf{I} : \boldsymbol{\Psi}_A \, \mathrm{d}\Omega = 0 \quad \forall \Psi_A \\ & \in X_A \subset L^2(\Omega)^{d\times d}. \end{aligned} \tag{12}$$

In the previous equations, we have adopted the notation $(\nabla \mathbf{v})_{ij} = \partial v_i / \partial x_j$. The viscoelastic stress and configuration tensors are related by Eq. (5).

Instead of solving the previous continuous problem, an approximate projected solution is sought in a finite-dimensional subspace $X_p^{n_p} \times X_v^{n_v} \times X_A^{n_A}$ of $X_p \times X_v \times X_A$, where $X_p^{n_p}$, $X_v^{n_v}$ and $X_A^{n_A}$ are, respectively, included into the space of polynomials of order less than or equal to n_p, n_v and n_A. In practice, some restrictions occur as far as the selection of the polynomial degrees is concerned. In particular, the inf–sup

condition imposes restrictions on the pressure subspace once the velocity subspace is prescribed, to prevent locking and spurious oscillation phenomena. In the spectral element context, the inf–sup condition is satisfied if $n_p = n_v - 2$ as emphasized by Maday and Patera [29]. No such condition has been clearly defined for the viscoelastic or configuration stress subspace although some relevant investigations have been carried out by Gerritsma and Phillips [24] in this direction. Van Kemenade and Deville [48] have observed numerically the influence of the viscoelastic stress approximation for a given benchmark problem (undulating channel), from which they provided some empirical criterion. The same subspace is selected for both configuration and viscoelastic stress tensors ($X_A = X_\tau$, $n_A = n_\tau$).

In our original spectral element method, two types of quadrature are used to approximate the integrals, namely the Gauss–Legendre and Gauss–Lobatto–Legendre quadratures [9]. The variables are approximated with expressions involving Lagrangian interpolation polynomials based on the quadrature collocation points [41]. The pressure grid using the Gauss–Legendre points is staggered with respect to the velocity and viscoelastic stress grid using the Gauss–Lobatto–Legendre points. An alternative that we have also implemented is to take the inner Gauss–Lobatto–Legendre velocity points as pressure points. By inner points, we mean points not comprising the boundaries of the elements. A study carried out by Van Kemenade and Deville [48] has shown that selecting the polynomial degrees for the velocity and viscoelastic stress approximations should be such that $n_v \leqslant n_\tau \leqslant n_v + 2$ for optimal results in the case of a viscoelastic flow through a corrugated tube. Gerritsma and Phillips [24] have considered the mixed formulation of the Stokes problem in terms of the velocity, pressure and extra-stress variables under a constrained minimization of the viscous stress tensor. They have found that the problem is well-posed as long as the stress approximation space contains polynomials of at least the same degree as the velocity. In most computations relative to viscoelastic flows with spectral element methods, the velocity and viscoelastic stress grids are taken to be the same. Furthermore, it has been recommended by the last two authors to use a discontinuous extra-stress approximation space (between elements) in order to satisfy a compatibility condition between the discrete velocity and stress spaces [23]. This idea can be extended to the viscoelastic stress when a viscoelastic problem is considered.

The discretization process leads to a set of equations, which can be cast in matrix form. Adopting the notations of Deville et al. [16], we obtain:

$$-D_k \underline{V}_k = 0, \quad k = 1, \ldots, d, \tag{13}$$

$$M \frac{\mathrm{d}\underline{V}_i}{\mathrm{d}t} = -Re\, C(\underline{V})\underline{V}_i + D_i^{\mathrm{T}} \underline{P} - R_\mu K_{ij} \underline{V}_j - VE_j \underline{T}_{ij} + (M_b)_{ij} \underline{S_b}_j. \tag{14}$$

The symbols $\underline{P}$, $\underline{V}_i$ and $\underline{T}_{ij}$ correspond to the vectors relative to the degrees of freedom for the pressure, velocity and viscoelastic stress components ($1 \leqslant i \leqslant d$, $1 \leqslant j \leqslant d$). The matrices M and K_{ij} are, respectively, diagonal mass and stiffness matrices. The discrete divergence operator is given by D_i and its transpose D_i^{T} yields the discrete gradient operator. The convection term is given by $C(\underline{V})\underline{V}_i$ where the nonlinear operator $C(\underline{V})$ depends on the velocity field.

The last two matrix operators are derived from the following integrals:

$$\int_\Omega \boldsymbol{\tau} \cdot \nabla \Psi_v \,\mathrm{d}\Omega \Rightarrow VE_j \underline{T}_{ij}, \quad \int_{\partial\Omega} (\boldsymbol{\sigma} \cdot \mathbf{n}) \cdot \Psi_v \,\mathrm{d}\Gamma \Rightarrow (M_b)_{ij} \underline{S_b}_j.$$

The constitutive equation in semi-discrete form reads:

$$\frac{We}{Re} \mathbf{Tr}(\underline{A}_{mn}) \frac{\mathrm{d}\underline{A}_{ij}}{\mathrm{d}t} + M \underline{A}_{ij} = NL_{ij}(\underline{A}_{mn}, \underline{V}_l), \tag{15}$$

where

$$NL_{ij}(\underline{A}_{mn}, \underline{V}_l) = -We[CA_{ij}(\underline{V}_l) - GA_{ij}(\underline{V}_l, \underline{A}_{mn}) - (GA)_{ij}^{\mathrm{T}}(\underline{V}_l, \underline{A}_{mn})].$$

Again, these operators written in matrix form are derived from the following integrals:

$$\begin{aligned}
&\int_\Omega \left(1-\frac{\mathrm{tr}(\mathbf{A})}{L_e^2}\right)\frac{\partial \mathbf{A}}{\partial t} : \Psi_A \,\mathrm{d}\Omega \Rightarrow \mathbf{Tr}(A_{mn})\,\frac{\mathrm{d}\underline{A}_{ij}}{\mathrm{d}t},\\
&\int_\Omega \mathbf{A} : \Psi_A \,\mathrm{d}\Omega \Rightarrow M\underline{A}_{ij},\\
&\int_\Omega \left(1-\frac{\mathrm{tr}(\mathbf{A})}{L_e^2}\right)[(\mathbf{v}\cdot\nabla)\mathbf{A}] : \Psi_A \,\mathrm{d}\Omega \Rightarrow CA_{ij}(\underline{V}_l),\\
&\int_\Omega \left(1-\frac{\mathrm{tr}(\mathbf{A})}{L_e^2}\right)[\nabla\mathbf{v}\cdot\mathbf{A}] : \Psi_A \,\mathrm{d}\Omega \Rightarrow GA_{ij}(\underline{V}_l,\underline{A}_{mn}),\\
&\int_\Omega f(\mathrm{tr}(\mathbf{A}))\mathbf{I} : \Psi_A \,\mathrm{d}\Omega \Rightarrow DT_{ij}(\underline{V}_l,\underline{A}_{mn})
\end{aligned} \tag{16}$$

The function $f(\mathrm{tr}(\mathbf{A}))$ is given by either Eq. (7) or (8). The symbol $\underline{A}_{ij}$ correspond to the vectors relative to the degrees of freedom for the configuration tensor components ($1 \leqslant i \leqslant d$, $1 \leqslant j \leqslant d$). Following Eq. (5), the configuration and viscoelastic stress vectors are related by a simple transformation:

$$\underline{T}_{ij} = \frac{1-R_\mu}{We}\,\frac{1}{1-(\underline{A}_{kk}/L_e^2)}\left(\underline{A}_{ij} - f(\underline{A}_{kk})\,\delta_{ij}\right), \tag{17}$$

where δ_{ij} is the usual Kronecker symbol.

The main problem with this formulation when applied to viscoelastic flows is that it may produce numerical instabilities when the Weissenberg number is increased. Therefore, stabilization techniques have sometimes to be introduced to remove these instabilities. We will introduce two of them, namely a filtering technique [33] and the so-called Discontinuous Elastic Viscous Stress Splitting (DEVSS) method [25], which have been found efficient in our computations when correct final steady-state solutions were only sought for.

3.2. Spectral mortar elements

Using spectral mortar elements [2,3] enables one to adapt locally the polynomial degree to regions with geometrical singularities or large gradients thus preventing the onset of numerical instabilities or improving the resolution in region where it is needed [1,50]. We have this type of elements in their functionally non-conforming version.

3.3. Filtering

We will present now a filtering technique proposed by Mullen and Fischer to stabilize the simulations of Newtonian flows at high Reynolds numbers with spectral elements [33]. The filter is applied after each time step on an element-by-element basis to both velocity and stress fields. The filter F_α is built as follows for a 2-D problem (and can be readily extended to the 3-D case):

$$F_\alpha = \alpha I_{N_x-Q_x,N_y-Q_y} + (1-\alpha)I_{N_x,N_y} \quad (0 \leqslant \alpha \leqslant 1), \tag{18}$$

where I_{N_x,N_y} is the identity operator, $I_{N_x-Q_x,N_y-Q_y}$ is the tensor product of the one-dimensional interpolation operators at the Gauss–Lobatto–Legendre nodes of order $N_x - Q_x$ and $N_y - Q_y$ in the x- and y-directions. The fields to which the filter is applied are supposed to be known at the Gauss–Lobatto–Legendre nodes of order N_x and N_y. The integers Q_x and Q_y are generally equal to 1 for Newtonian fluids. The filter operator tends to damp high-frequency oscillations since the nodal basis points of order N interlace those of order $N - Q$.

3.4. DEVSS method

The DEVSS method has been proposed by Guénette and Fortin [25]. In this formulation, the rate-of-deformation tensor $\mathbf{D}_X$ is usually considered as an additional unknown. Therefore, an additional equation with respect to the Galerkin formulation is introduced to set the approximation space for $\mathbf{D}_X$:

$$\int_\Omega \left[\mathbf{D}_X - \frac{1}{2}\left(\nabla\mathbf{v} + (\nabla\mathbf{v})^{\mathrm{T}}\right)\right] : \Psi_D \,\mathrm{d}\Omega = 0 \quad \forall \Psi_D \in X_D \subset L^2(\Omega)^{d\times d}. \tag{19}$$

As opposed to the classical Elastic Viscous Stress Splitting (EVSS) method, no explicit change of variable is performed in the constitutive equation, therefore the viscoelastic stress remains the stress variable. The continuity and constitutive equations remain unchanged (Eqs. (9) and (12)) with respect to the standard Galerkin formulation. The weak form of the momentum equation becomes:

$$B_{\mathrm{DEVSS}}(p, \mathbf{v}, \boldsymbol{\tau}, \Psi_v) = B(p, \mathbf{v}, \boldsymbol{\tau}, \Psi_v) + B_{\mathrm{add}}(p, \mathbf{v}, \boldsymbol{\tau}, \Psi_v) = 0 \quad \forall \Psi_v \in X_v \subset H^1(\Omega)^d, \tag{20}$$

where $B(p, \mathbf{v}, \boldsymbol{\tau}, \Psi_v)$ is given by Eq. (10) and $B_{\mathrm{add}}(p, \mathbf{v}, \boldsymbol{\tau}, \Psi_v)$ by the following equation:

$$B_{\mathrm{add}}(p, \mathbf{v}, \boldsymbol{\tau}, \Psi_v) = 2R'_\mu \int_\Omega (\mathbf{D} - \mathbf{D}_X) : \nabla\Psi_v \,\mathrm{d}\Omega. \tag{21}$$

The quantities $\mathbf{D}$ and $\mathbf{D}_X$ are, respectively, the continuous and approximated rate-of-deformation tensors. The arbitrary parameter R'_μ can be considered as an additional viscosity.

The term $2R'_\mu(\mathbf{D} - \mathbf{D}_X)$ is introduced in the momentum equation for stabilization purpose. If the UCM model is used, there is no viscous term in this equation. Introduction of this auxiliary viscous term enables to recover the elliptic character of the momentum equation. This term vanishes when the mesh is refined or when the approximation space of the rate-of-deformation tensor is rich enough. For the Oldroyd-B model, it enables to increase the contribution of the Laplacian (viscous) term $(R_\mu + R'_\mu)\int_\Omega(\nabla\mathbf{v}) : \nabla\Psi_v \,\mathrm{d}\Omega$ with respect to the extra-stress term $(\int_\Omega(\boldsymbol{\tau} - 2R'_\mu\mathbf{D}_X) : \nabla\Psi_v \,\mathrm{d}\Omega)$, which helps to stabilize the computation.

4. Time discretization

The semi-discrete set of nonlinear ordinary equations (13)–(15) must still be approximated in time in order to generate the time marching scheme. However, a careful inspection of this set of equations shows that the coupled solution, especially for a three-dimensional problem, seems to be out of reach, even on the most powerful supercomputers. Therefore, it is advisable to resort to splitting techniques to decouple velocity–pressure and stress computations.

Iterative solvers are used to obtain numerical solutions of the linearized systems appearing once the problem is discretized in space and time with reduced computer memory requirements when the problem size is not small. Various approaches can be used to solve the systems of equations.

4.1. Decoupled techniques

The present decoupled technique builds upon classical time-dependent Navier–Stokes solvers. The extension to non-Newtonian fluids is based on the explicit time integration of the constitutive relation. Once the viscoelastic stress tensor is known at the new time level, it is incorporated in the Navier–Stokes equations as a source term.

More precisely, our fully decoupled approach consists in solving separately the mass–momentum and constitutive equations. The constitutive equation is integrated at time step $n+1$ for the configuration

tensor while using velocity gradient terms obtained at previous time steps. The viscoelastic stress tensor computed by its expression in terms of the configuration tensor is then inserted as a source term into the momentum equation. The mass–momentum system of equations is then solved for the velocity and pressure at the new time step $n+1$ using a classical technique for the Navier–Stokes problem [14,15]. Such stress–velocity decoupled iterative techniques are cheap in terms of CPU time, but they may suffer from poor convergence properties. Various schemes can be used for the temporal discretization of Eqs. (13)–(15). We have used in particular a backward differentiation formula (BDF) for implicit terms and the extrapolation scheme (EX) for explicit terms [26], which leads to the following system of equations. In order to simplify the notation with respect to Eqs. (13)–(15), we introduce a shorthand notation where $\underline{V}$, $\underline{P}$, $\underline{A}$ and $\underline{T}$ represent the full vectors of all velocity pressure, configuration and viscoelastic stress nodal unknowns. The block diagonal matrices $\mathbf{M}$ and $\mathbf{K}$ are, respectively, composed with d block matrices M and K. The matrix $\mathbf{D}$ corresponds to the full divergence operator and $\mathbf{D}^{\mathrm{T}}$ to the full gradient operator. The symbol $\mathbf{Tr}$ is relative to the trace term in Eq. (15). The system of discretized equations reads:

$$-\mathbf{D}\underline{V}^{n+1} = 0, \tag{22}$$

$$\left(\frac{\beta_{s_i}}{\Delta t}\right)\mathbf{M}\underline{V}^{n+1} - \mathbf{D}^{\mathrm{T}}\underline{P}^{n+1} + R_\mu \mathbf{K}\underline{V}^{n+1} = \frac{1}{\Delta t}\sum_{q=1}^{s_i}\beta_{s_i-q}\mathbf{M}\underline{V}^{n+1-q} - \sum_{r=0}^{s_e-1}\alpha_r Re\,\mathbf{C}(\underline{V}^{n-r}) - \mathbf{VE}\,\underline{T}^{n+1} + \mathbf{M_b}\underline{S_b}^{n+1}, \tag{23}$$

$$\underline{T}^{n+1} = \mathbf{TA}\,\underline{A}^{n+1}, \tag{24}$$

$$\left(\frac{We}{Re\,\Delta t}\beta_{s_i}\mathbf{Tr} + \mathbf{M}\right)\underline{A}^{n+1} = \frac{We}{Re\,\Delta t}\sum_{q=1}^{s_i}\beta_{s_i-q}\mathbf{Tr}\underline{A}^{n+1-q} + \sum_{r=0}^{s_e-1}\alpha_r\mathbf{NL}(\underline{A}^{n-r}\underline{V}^{n-r}), \tag{25}$$

where an extrapolation method of order s_e has been used to determine the value of the nonlinear term at time step $n+1$. The associated BDF scheme is of order s_i. The coefficients α_i and β_j are dependent of the orders of each method, e.g., for a BDF2/EX2 scheme: $\alpha_0 = 2$, $\alpha_1 = -1$, $\beta_0 = \frac{1}{2}$, $\beta_1 = -2$, $\beta_2 = \frac{3}{2}$. Eq. (24) is a short-hand notation for representing Eq. (17).

Since the nonsymmetric (nonlinear) terms in Eqs. (22)–(25) are located in the right-hand sides, cheap preconditioned conjugate gradient solvers can be used to solve the resulting system for the unknowns at the grid points. Eq. (25) is readily solved since there are no implicit terms with non-trivial matrix operators.

The efficiency of this decoupled method depends critically on the availability of an efficient and robust solver for the underlying Stokes problem at each time step. Our approach consists of solving the mass–momentum set of Eqs. (22) and (23) with an efficient solver as designed by Couzy [14,15] for Newtonian flows, which can be easily extended to viscoelastic flows by simply adding the divergence term corresponding to the viscoelastic stress tensor as a source term in the momentum equation. The set of mass–momentum equations is treated via a generalized block LU decomposition with pressure correction, which can be summarized by the following steps:

Step 1: Compute the tentative velocity vector $\underline{V}^*$ by solving the equation:

$$\mathbf{H}\underline{V}^* = \underline{F} + \mathbf{D}^{\mathrm{T}}\underline{P}^n, \tag{26}$$

which is a short notation for Eq. (23) where the pressure term has been shifted to the right-hand side. The Helmholtz operator matrix $\mathbf{H}$ comprehends both mass and Laplacian contributions while all other terms including the convective one are in the right-hand side vector $\underline{F}$:

$$\mathbf{H} = \left(\frac{\beta_{s_i}}{\Delta t}\right)\mathbf{M} + R_\mu \mathbf{K}, \tag{27}$$

$$\underline{F} = \frac{1}{\Delta t}\sum_{q=1}^{s_i} \beta_{s_i - q}\mathbf{M}\underline{V}^{n+1-q} - \sum_{r=0}^{s_e-1} \alpha_r Re\,\mathbf{C}(\underline{V}^{n-r}) - \mathbf{VE}\,\underline{T}^{n+1} + \mathbf{M_b}\,\underline{T_b}^{n+1}. \tag{28}$$

Step 2: Solve for the pressure

$$-\mathbf{DQD}^{\mathrm{T}}\underline{\Delta P}^{n+1} = \frac{\beta_{s_i}}{\Delta t}\mathbf{D}\underline{V}^*, \tag{29}$$

$$\underline{P}^{n+1} = \underline{P}^n + \underline{\Delta P}^{n+1} - R_\mu \mathbf{D}\underline{V}^*. \tag{30}$$

The last term in Eq. (30) has been introduced to obtain an overall consistent scheme as suggested by Timmermans et al. [47].

Step 3: Compute the final velocity at step $n+1$ after a pressure correction:

$$\underline{V}^{n+1} = \underline{V}^* + \frac{\Delta t}{\beta_{s_i}}\mathbf{QD}^{\mathrm{T}}\underline{\Delta P}^{n+1}.$$

The choice of the matrix $\mathbf{Q}$ is critical. If one sets:

$$\mathbf{Q} = \mathbf{H}^{-1} \tag{31}$$

one gets back the Uzawa technique or if one writes an approximation of $\mathbf{H}^{-1}$, e.g., for a BDF2/EX2 scheme:

$$\mathbf{Q} = \frac{\Delta t}{\beta_2}\mathbf{M}^{-1} - R_\mu\left(\frac{\Delta t}{\beta_2}\right)^2(\mathbf{M}^{-1}\mathbf{K})\mathbf{M}^{-1} + (R_\mu)^2\left(\frac{\Delta t}{\beta_2}\right)^3(\mathbf{M}^{-1}\mathbf{K})^2\mathbf{M}^{-1} \tag{32}$$

as proposed by Perot [37] one obtains a fourth-order approximation in time. If accuracy in time is limited to second order, only the first term in the previous expansion needs to be retained. Efficient preconditioners for the iterative solver of the pressure step Eq. (29), which is by far the most expensive one in terms of CPU time, have been prescribed by Couzy and Deville [13] and Couzy [14,15]. Simple diagonal preconditioners are used for the two velocity steps.

4.2. Fully coupled technique

In the coupled approach, the three discretized partial differential equations are solved altogether for all the unknowns from time step n to time step $n+1$. Generally, coupled methods are more stable than decoupled ones but the required computer ressources (memory and CPU time) are more stringent. The full nonlinear coupled problem is generally solved by a succession of Newton iterations applied once the entire set of equations is discretized. The computer storage to set up and invert the Jacobian matrix for the Newton iteration is very demanding. Newton schemes provide quadratic convergence and therefore, few iterations are needed to reach a solution provided the initial guess is good enough. The presence of implicit terms when solving the constitutive equation implies that the resulting matrix after spatial discretization is not symmetric as opposed to fully decoupled methods. This means that the cheap preconditioned conjugate gradient methods cannot be used. Efficient preconditioning is an important issue for iterative methods to solve linear systems with non-symmetric matrices and especially for the GMRES method [42]. Good preconditioning is needed to obtain fast convergence otherwise the cost becomes rapidly prohibitive. There

is no explicit treatment of some operators in these schemes, which makes them a priori less sensitive to time-dependent numerical instabilities and avoids limitations due to Courant-type criteria on the time step.

The set of semi-discrete Eqs. (13)–(15) can be written in simple form:

$$\mathscr{M}\frac{\mathrm{d}\underline{X}}{\mathrm{d}t}+\underline{G}(\underline{X})=0, \tag{33}$$

where $\underline{X}$ is the vector containing the unknowns at the collocation points:

$$\underline{X}^{\mathrm{T}}=\left[\underline{P}^{\mathrm{T}},\underline{V}^{\mathrm{T}},\underline{T}^{\mathrm{T}},\underline{A}^{\mathrm{T}}\right]. \tag{34}$$

Using the notations introduced in Eqs. (13)–(15), the expressions for $\mathscr{M}$ and $\underline{G}(\underline{X})$ are

$$\mathscr{M}=\begin{bmatrix}0&0&0&0\\0&M&0&0\\0&0&0&\frac{We}{Re}M\\0&0&M&0\end{bmatrix}, \tag{35}$$

$$\underline{G}(\underline{X})=\begin{bmatrix}D\underline{V}\\-D^{\mathrm{T}}\underline{P}+Re\,\underline{C}(\underline{V})+R_{\mu}K\,\underline{V}+VE\,\underline{T}-M_b\,\underline{S}_b\\-M\,\underline{A}+NL(\underline{A},\underline{V})\\TA(\underline{A})\end{bmatrix}. \tag{36}$$

Various time discretization schemes have been proposed in the literature for this type of viscoelastic problems. One of the simplest is the trapezoidal rule or Crank–Nicolson scheme, which is second-order accurate and leads to:

$$\hat{\underline{G}}(\underline{X}^{n+1})=2\mathscr{M}(\underline{X}^{n+1}-\underline{X}^{n})+\Delta t(\underline{G}(\underline{X}^{n+1})+\underline{G}(\underline{X}^{n}))=\underline{0}. \tag{37}$$

This equation is solved by a classical Newton method, i.e., by solving iteratively or directly the following equation:

$$\mathbf{J}_{\hat{\underline{G}}}(\underline{X}^{n})\delta\underline{X}^{n}=-\hat{\underline{G}}(\underline{X}^{n}), \tag{38}$$

where $\mathbf{J}_{\hat{\underline{G}}}$ is the Jacobian of $\hat{\underline{G}}$: $\mathbf{J}_{\hat{\underline{G}}}(\underline{X}^{n})=(\partial\hat{\underline{G}}/\partial\underline{X})(\underline{X}^{n})$ and $\delta\underline{X}^{n}=\underline{X}^{n+1}-\underline{X}^{n}$. A slightly more sophisticated alternative is to use a predictor–corrector method with adaptive time step as suggested by Bodart and Crochet [5]. We have considered both alternatives with a direct solver since we have only dealt with problems of small size.

4.3. Other methods

Several mixed and semi-implicit methods have been proposed in the literature to get more efficient solvers while preserving a high degree of stability and the possibility to use large time steps, e.g. [34]. We have actually implemented many more techniques than the ones presented in the previous sections. For the sake of brevity, we will not present them in details here since they have not brought substantial improvement in terms of stability of the computations with the Oldroyd-B model. In particular, an attractive alternative to the extrapolation method to determine the explicit terms in Eqs. (23)–(25) is the operator integration factor splitting (OIFS) technique [30]. It has been applied with success to the simulation of Newtonian fluids, e.g., [14]. However, we have not found that it was superior to the BDF/EX method presented in the Section 4.1 in terms of stability for simple flows of viscoelastic fluids. Among other methods that we have tested in the context of decoupled techniques, let us mention another operator

splitting method, namely the θ-method [46], predictor–corrector techniques at each time step, implicit and explicit Runge–Kutta methods applied to the Oldroyd-B constitutive equation.

5. Test problems

In order to analyze the relevance of the proposed time and space discretizations, we introduce a simple test case (time-dependent Poiseuille flow) for which an analytical solution is available for comparison and a more complicated benchmark problem (flow through a two-dimensional planar contraction).

5.1. Planar Poiseuille flow

We have simulated steady and time-dependent Poiseuille flows. A constant non-zero pressure gradient is imposed to the flow if the generation of a steady flow is expected at large times or that the gradient is removed when starting from steady-state conditions (at large times, the velocity and viscoelastic stress decay to zero values).

In the case of Poiseuille flows (see Fig. 1), the continuity, momentum and constitutive equations (1), (2) and (6) can be simplified since all unknowns depend only on the transverse coordinate y and the transverse component of the velocity v_y vanishes as well as all convective terms. Analytical solutions providing the velocity field are available for this type of flow for an Oldroyd-B fluid as reported in [49]. We briefly recall here the formulae for both flow generation and decay.

The expressions for the velocity components are:

$$v_x(y,t) = V_{\max}\left[4(1-y)y - 32\sum_{n=1}^{\infty}\frac{\sin(Ny)}{N^3}\exp\left\{\frac{-\alpha_N t}{2S_1}\right\}G_N(t)\right] \quad \text{(Generation)} \tag{39}$$

with $N = (2n-1)\pi$, $\alpha_N = 1 + S_2N^2$, $S_1 = We/Re$, $S_2 = R_\mu S1$.

$$v_x(y,t) = V_{\max}\left[32\sum_{n=1}^{\infty}\frac{\sin(Ny)}{N^3}\exp\left\{\frac{-\alpha_N t}{2S_1}\right\}G_N(t)\right] \quad \text{(Decay)}, \tag{40}$$

$$v_y(y,t) = 0.0, \tag{41}$$

where the function $G_N(t)$ is given by

$$G_N(t) = \cosh\left(\frac{\beta_N}{2S_1}t\right) + \frac{1+N^2(S_2-2S_1)}{\beta_N}\sinh\left(\frac{\beta_N}{2S_1}t\right) \tag{42}$$

with $\beta_N = \sqrt{(1+S_2N^2)^2 - 4S_1N^2}$.

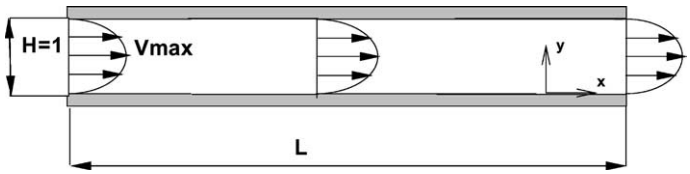

Fig. 1. Poiseuille flow in a planar channel.

The maximum velocity $V_{\max}$ is related to the pressure gradient along the channel by $V_{\max} = -(1/8)(\partial p/\partial x)$.

The viscoelastic stress component τ_{xy} can then be obtained by integrating the momentum equation relative to the first component v_x with respect to y:

$$\tau_{xy}(y,t) = V_{\max}\left[-4(1-R_\mu)(2y-1) + 32\sum_{n=1}^{\infty}\frac{\cos(Ny)}{N}\exp\left\{\frac{-\alpha_N t}{2S_1}\right\}H_N(t)\right] \quad \text{(Generation)}, \tag{43}$$

$$\tau_{xy}(y,t) = V_{\max}\left[-32\sum_{n=1}^{\infty}\frac{\cos(Ny)}{N}\exp\left\{\frac{-\alpha_N t}{2S_1}\right\}H_N(t)\right] \quad \text{(Decay)}, \tag{44}$$

where the function $H_N(t)$ is related to the function $G_N(t)$ by:

$$H_N(t) = \left(\frac{R_\mu}{N} - \frac{(\alpha_N/2S_1)}{N^3}\right)G_N(t) + \frac{1}{N^3}G'_N(t). \tag{45}$$

The other non-zero component τ_{xx} is obtained by integrating the constitutive equation involving the partial derivative of τ_{xx} with respect to time:

$$\tau_{xx} = 2\exp\left\{-\frac{Re\,t}{We}\right\}\int_0^t \tau_{xy}(y,u)\frac{\partial v_x}{\partial y}(y,u)\exp\left\{\frac{Re\,u}{We}\right\}\mathrm{d}u. \tag{46}$$

When steady-state conditions are reached, the flow unknowns are given by

$$v_x(x,y,z) = 4V_{\max}y(1-y), \tag{47}$$
$$v_y(x,y,z) = 0, \tag{48}$$
$$p(x,y,z) = -8V_{\max}x + p_0, \tag{49}$$
$$\tau_{xx}(x,y,z) = 32V_{\max}^2 We(1-R_\mu)(1-2y)^2, \tag{50}$$
$$\tau_{xy}(x,y,z) = 4V_{\max}(1-R_\mu)(1-2y), \tag{51}$$
$$\tau_{yy}(x,y,z) = 0, \tag{52}$$

where p_0 is the pressure at the channel inflow section.

Expressions for the UCM model are obtained by setting $R_\mu = 0$.

For other fluids like, e.g., FENE-P, no such simple expressions can be derived analytically. However the constitutive equation becomes a set of nonlinear equations where all derivatives of the configuration tensor have disappeared. In addition, the derivatives of the velocity can also be replaced by expressions involving only the components of **A**. This set can be readily solved by Newton's method.

Starting from Eqs. (1), (2) and (5)–(7), one obtains

$$KA_{xx} - 2\frac{WeK}{R_\mu}A_{xy}\left[-4V_{\max}(2y-1)\left(1-\frac{A_{xx}+A_{yy}}{L_e^2}\right) - \frac{1-R_\mu}{We}A_{xy}\right] - 1 + \frac{A_{xx}+A_{yy}}{L_e^2} = 0, \tag{53}$$

$$A_{xy} - \frac{We}{R_\mu}A_{yy}\left[-4V_{\max}(2y-1)\left(1-\frac{A_{xx}+A_{yy}}{L_e^2}\right) - \frac{1-R_\mu}{We}A_{xy}\right] = 0, \tag{54}$$

$$KA_{yy} - 1 + \frac{A_{xx}+A_{yy}}{L_e^2} = 0. \tag{55}$$

The viscoelastic stress components are obtained from Eqs. (5) and (7). It must be noted that the last component of the viscoelastic stress tensor τ_{yy} is equal to zero.

The computed values of the velocity and configuration tensor are used to prescribe inflow and outflow Dirichlet conditions in problems with closed boundaries as explained in Section 5.2.2.

5.2. Flow through a two-dimensional planar contraction

As an example with a non-trivial geometry, we have selected here the flow of a FENE-P fluid through an abrupt four-to-one planar two-dimensional contraction. Corresponding numerical results will be deferred until Section 6.2. The types of boundary conditions that we have used in simulations are described hereafter.

5.2.1. Geometry

The geometry of the contraction is shown in Fig. 2, where D_u, D_d and R_c are, respectively, the heights of the upstream and downstream channels and the arc radius of the re-entrant corner (close to the downstream channel). Simulations with either sharp or rounded corner have been carried out. Rounding-off the corner induces the effect of removing the strong viscoelastic stress singularity that is otherwise present in the flow.

5.2.2. Boundary conditions

As opposed to Newtonian flows, no clearly established rule for prescribing boundary conditions exists for viscoelastic flows. A common practice reported in many papers is to impose Dirichlet conditions for the velocity on the whole domain boundary and for the configuration tensor at the inflow boundary. Dirichlet conditions at inflow are prescribed by imposing the values obtained by computing $\mathbf{v}$ and $\mathbf{A}$ in a Poiseuille flow with the same channel height D_u as described in Section 5.1. We have also considered a more suitable alternative, which consists of imposing the same type of conditions for the configuration tensor, Dirichlet conditions for the velocity everywhere except at the outflow boundary, where natural conditions are applied. By natural boundary conditions, we mean that the surface integrals involved in the discretized momentum equation (see Eq. (10)) are evaluated in terms of the unknowns at the outflow boundary nodes

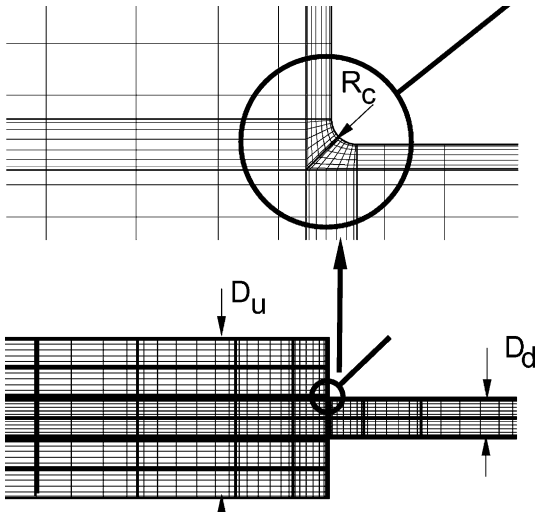

Fig. 2. Typical geometry and mesh of the two-dimensional planar contraction.

(p, $\mathbf{v}$ and $\boldsymbol{\tau}$) together with the volume integrals [36]. This last type of boundary conditions was found slightly better in terms of accuracy or convergence towards steady-state of the solution in most of our computations. It has been also used by Bodart and Crochet for simulating the time-dependent flow of viscoelastic fluids with finite elements [5]. Since we are using a classical spectral element method with the $\mathbb{P}_N - \mathbb{P}_{N-2}$ formulation for the velocity and pressure [29], no explicit boundary condition is imposed on the pressure since no pressure grid point lies on the boundary of the computational domain. All the plots shown in the following sections correspond to natural outflow boundary condition.

6. Results

This section presents the results that have been obtained on two benchmark problems: the two-dimensional flows of viscoelastic fluids through a planar channel and a four-to-one two-dimensional abrupt contraction.

Simulations relative to the contraction have produced results that are in good agreement with the literature [39] over a significant range of Weissenberg numbers, thus showing the relevance of our computational method. However, long-term numerical instabilities appear at a critical Weissenberg number for a given mesh and result in the divergence of the simulations. The same observations are valid for the simpler Poiseuille flow benchmark problem. A more detailed and systematic investigation of the source of these instabilities can be carried out in that case.

6.1. Poiseuille unsteady flows of an Oldroyd-B fluid

An obvious and relevant test at this stage is to consider the Poiseuille unsteady flows (generation and decay) of an Oldroyd-B fluid presented in Section 5.1. For a 4×2 equally spaced element discretization with polynomial orders, respectively, equal to 4 and 5 in the streamwise and cross-stream directions using the BDF2/EX2 algorithm. Fig. 3 shows the typical variations of the non-zero velocity and viscoelastic stress components when the flow generation and decay are enforced. The analytical curves have not been shown since they were almost undistinguishable from the computed ones, except for a few time steps when the flow regime was imposed. The time step used for the simulations is set equal to 0.01.

The DEVSS and filtering technique presented in Sections 3.3 and 3.2 helped in stabilizing the simulations (higher We could be reached for a given mesh) but at the expense of increasing the error during the transient phase. The global variations of the non-zero velocity and viscoelastic stress components due to the elastic effects in the flow were reproduced by the simulations. However, the relative maxima on the curves shown in Fig. 3 were (slightly) shifted and their amplitude (weakly, i.e., typically a few percents) modified although final steady-state values were obtained with good accuracy. This raises the question of the validity of these techniques to simulate transient flows of viscoelastic fluids.

6.2. Flow through a planar four-to-one abrupt contraction

The goal of this section is not to present detailed results relative to the flow through a planar contraction but to show that satisfactory results can be obtained with the spectral element method that we have described in Section 3.1 using the decoupled technique of Section 4.1 for a problem with a non-trivial geometry. We will also show typical numerical instabilities that occur when the Weissenberg number is increased. Understanding the source of these instabilities in an uneasy task that we have tried to investigate on the simpler Poiseuille flow problem.

Simulations based on the computational algorithm described in Section 4.1 have been carried out with various fluid models for the four-to-one two-dimensional abrupt contraction using either the natural or full Dirichlet boundary conditions described in Section 5.2.2. Zero-field initial conditions have been imposed

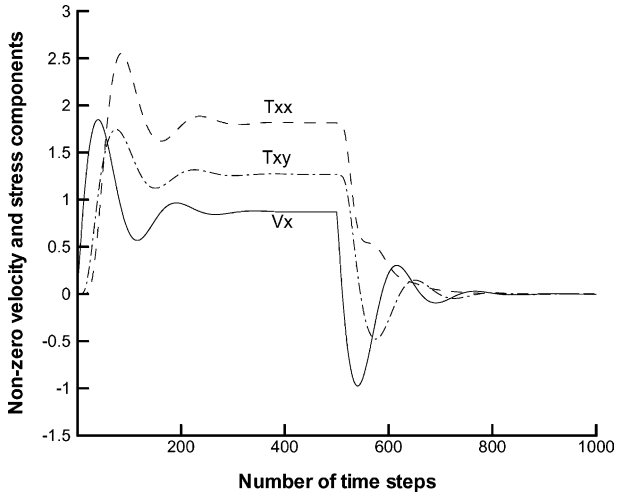

Fig. 3. Generation and decay of planar Poiseuille flow of an Oldroyd-B fluid for $We = 0.5$.

for **v** and **A**. The velocity field develops rapidly in the first stage of the simulation until it remains almost constant. The viscoelastic stress components are converging towards steady-state in a much slower way.

Fig. 4 shows plots of typical streamlines and contour lines of the pressure and viscoelastic stress components for a FENE-P fluid. The corresponding fluid parameters are $Re = 1$, $We = 8.0$, $L_e^2 = 6.0$, $R_\mu = \frac{1}{9}$. Elastic effects can clearly be observed as large vortices are developed near the vertical contraction plane. Such vortices are not visible with a similar plot scale for Newtonian fluids. The maxima of the viscoelastic stress components are observed near the re-entrant corner. The ratio of the its arc radius R_c over the downstream channel height D_d is equal to 0.05. A uniform polynomial order equal to 7 has been set over most of the elements except in the vicinity of the re-entrant corner where it has been decreased to 4 in order to improve numerical stability. Spectral mortar elements were therefore used in that region. Second-order schemes for the linear (BDF2) and nonlinear (EX2) operators in Eqs. (23) and (25) have been used for the simulation as well as a second-order fractional step method with pressure correction to solve the mass–momentum set of equations as described in Section 4.1. The simulations have been carried out without resorting to any stabilization technique.

For a given mesh and geometry, instabilities occur above a critical value of the Weissenberg number. Fig. 5 shows the typical nascent instabilities in the τ_{xx} contour plot that are present a few time steps before the simulation diverges. The corresponding parameters are $Re = 1$, $We = 4.0$, $L_e^2 = 10.0$, $R_\mu = \frac{1}{9}$ for the FENE-P fluid and $R_c = 0.025 D_d$ for the arc radius.

No such instabilities are observed for a Newtonian fluid for this value of the Reynolds number. Instabilities stem from the hyperbolic character of the constitutive equation, the presence of time derivatives and the decoupling of the velocity-pressure and viscoelastic stress solvers. This will be analyzed in more details in Section 6.3.

Clearly, the stability of the simulation can be improved by adapting the mesh and element polynomial orders. Natural boundary conditions were found better than Dirichlet conditions at outflow in terms of stability since the critical Weissenberg number was larger. As expected, the maximum stress level near the re-entrant corner is reduced as the arc radius is increased, which allows to carry out stable simulations at higher Weissenberg numbers. Among the fluid parameters, the extensibility length L_e and the viscosity ratio R_μ have a strong influence on the critical value We_{crit} of We for a given mesh. The effects of elasticity are enhanced if R_μ decreases since this parameter is the ratio of the solvent Newtonian viscosity over the total

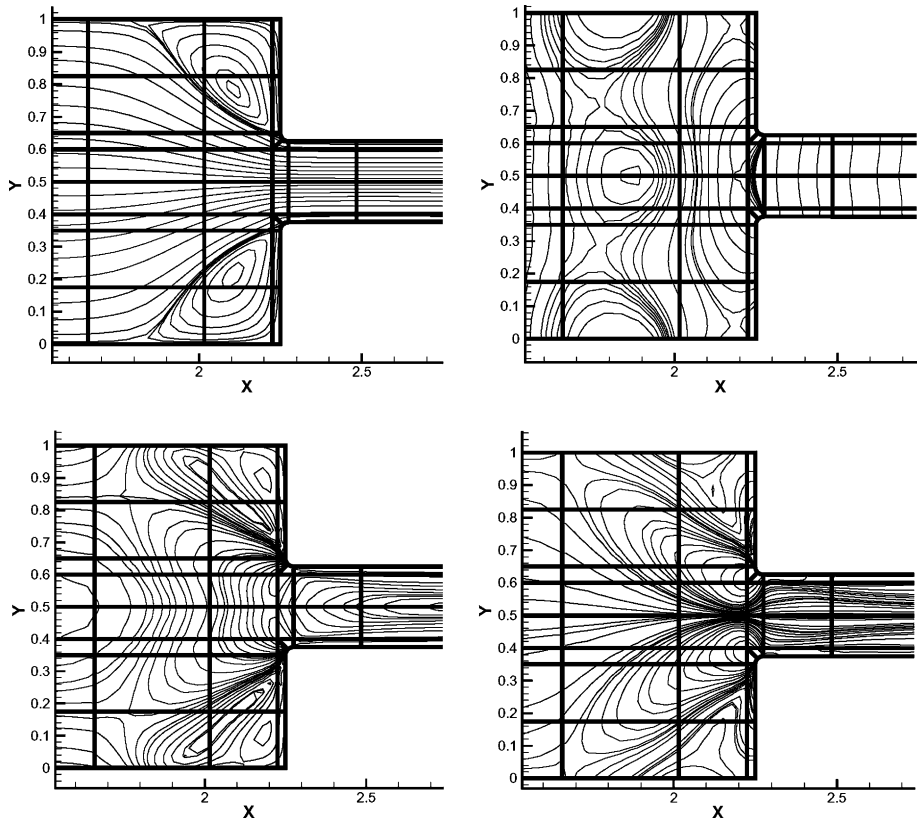

Fig. 4. Typical streamlines (upper left), pressure (upper right), τ_{xx} (lower left) and τ_{xy} (lower right) contour lines of a FENE-P fluid in a 4:1 abrupt planar contraction.

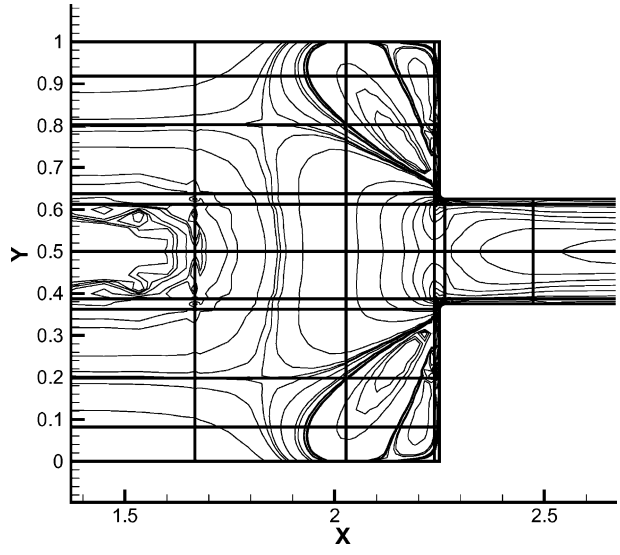

Fig. 5. Nascent instabilities in the τ_{xx} contour plot at a given Weissenberg number ($We = 4.0$).

viscosity. The maximum value of the viscoelastic stress components increases with L_e. Consequently, We_{crit} decreases with R_μ and L_e^{-1}. The stiff Oldroyd-B model corresponds to $L_e \to \infty$.

6.3. Steady Poiseuille flows

We will now present a detailed investigation of the influence of the geometrical and physical parameters on the numerical stability of our computational method for the simpler Poiseuille flow of FENE fluids (including the Oldroyd-B fluid as the limit case). Most of the contents of this section is dedicated to the convergence towards steady-state. The generation and decay of Poiseuille flows are also considered as test cases to check the ability of the algorithm to describe correctly transient flows. Let us recall here that we have checked that none of the instabilities described in this section are present if a Newtonian fluid is considered.

6.3.1. Oldroyd-B model

First, we will present results for the decoupled technique presented in Section 4.1 so as to emphasize the problems that arise when using time integration even for solving simple steady problems. Specific aspects due to the spectral element method will be underlined as well as possible stabilization techniques. Then, it will be shown that these problems are not solely a consequence of using a decoupled scheme but also exist with more robust algorithms.

Throughout this section, we will refer to x and y, respectively, as the streamwise and cross-stream directions, L and H as the channel length and height, NE_x and NE_y as the number of spectral elements in the two directions, N_x and N_y as the corresponding polynomial orders (kept fixed for all elements). We will present here only plots of the relative error of the velocity field $\|v - v_{analytical}\|/\|v_{ref}\|$ based on the Euclidean norm versus time for the sake of simplicity. Similar plots are obtained for the viscoelastic stress tensor. The amplitude of the Poiseuille flow is selected such that the channel flow rate $\int_0^H v_x(y')\,dy'$ is equal to one. All data plots shown in this paper correspond to a time step equal to 0.01 (unless specified), a Reynolds number Re equal to 1, a unit channel height H and a viscosity parameter R_μ equal to $\frac{1}{9}$, which is a value commonly used in benchmark problems. Simulations with various values of these parameters have been carried out but their corresponding results are not given here since they are in qualitative agreement with those described in the following subsections. Unless otherwise specified, the polynomial orders N_x and N_y have been, respectively, set equal to 4 and 5.

We have used various initial conditions varying from zero-field values for all flow variables to the full analytical prescription of the steady flow. The last option was used to check that the numerical instabilities were not due to initial conditions that were not close enough to the steady flow solution to obtain convergence. When dealing with more complex flows and a coupled equation solver, it is generally necessary to use the solution of a previous run at a slightly lower Weissenberg number to get convergence. This was not the case for the simple flows that we tested as well as for the contraction problem. Most of the plots have been produced using the simple Galerkin formulation and the computational algorithm described in Section 4.1 (decoupled technique with a BDF2/EX2 time scheme, cf. Eqs. (22)–(25)).

When selecting the exact steady-state expression as initial condition, convergence of the numerical solution towards steady-state is obtained at the first step, i.e., the relative errors of the velocity, viscoelastic stress and pressure is very low (typically 1.0e − 12). A striking point is that, above a given Weissenberg number, these errors increase with the number of steps at an exponential rate which can be easily identified by a straight line in a semi-log plot, thus revealing the presence of a dominant mode corresponding to a real positive eigenvalue as shown in Fig. 7.

Figures shown in the rest of this section correspond to initial conditions prescribed by analytical expressions of the steady flow. Values of the unknown fields at the first time step (if a BDF2 scheme is selected) are computed by a Crank–Nicolson starter scheme. The BDF2/EX2 requiring expressions of the

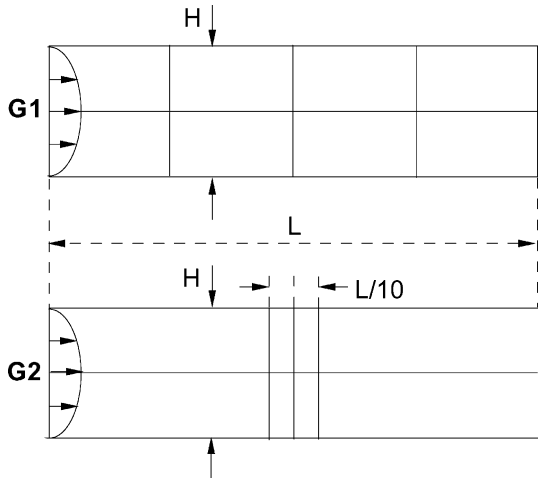

Fig. 6. Poiseuille flow in a planar channel with typical mesh decomposition ($NE_x = 4, NE_y = 5$).

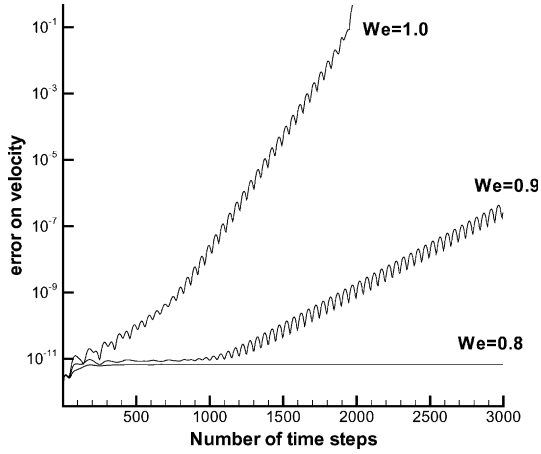

Fig. 7. Typical variation of the relative error of the velocity $\|v - v_{\text{analytical}}\|_E / \|v_{\text{analytical}}\|_E$ (Euclidean norm) vs number of time steps for the Poiseuille flow of an Oldroyd-B fluid with exact steady-state initial conditions.

fields at the two previous time steps can then used for all the following steps. This starting process is responsible for the initial jump and oscillation growth during the first time steps in the following error plots.

Typical instabilities for an Oldroyd-B fluid are shown in Fig. 8, which corresponds to geometries G1 and G2 illustrated in Fig. 6. The curves are relative to various Weissenberg numbers for the two domain decompositions. G1 corresponds to a discretization with elements of equal size whereas G2 corresponds to elements with variable size in the streamwise direction. Even though there is hardly no difference at low values of *We*, the mesh discretization has a non-negligible effect on the convergence towards the steady-state solution.

For a discretization with a fixed number of elements in both directions, computations with various domain lengths have shown that instabilities occur when the length is reduced below a critical value at a given Weissenberg number. This has been observed by other groups using for example finite elements, e.g., [43]. It has been suggested that this problem might be due to unsuitable boundary conditions at the channel

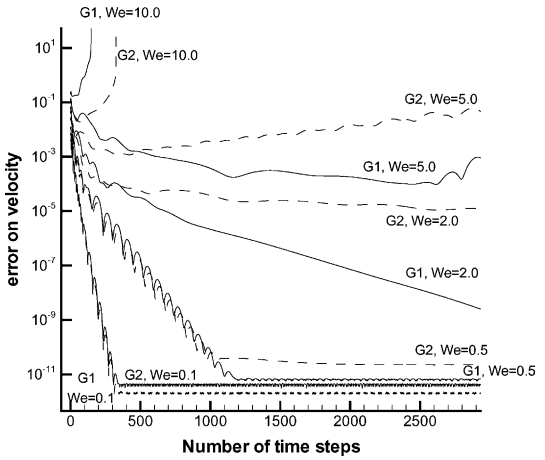

Fig. 8. Typical variation of the relative error of the velocity $\|v - v_{\text{analytical}}\|_E / \|v_{\text{analytical}}\|_E$ (Euclidean norm) vs number of time steps for the Poiseuille flow of an Oldroyd-B fluid (see text for initial conditions and Fig. 6 for configurations G1 and G2, $L = 64$).

exit. In addition to the boundary conditions described in Section 5.2.2, we have also implemented pseudo-periodic boundary conditions by setting the velocity in the inflow section equal to the velocity in the outflow section at the previous time step. This has not led to any substantial improvement.

Let us emphasize that the limiting values of the Weissenberg number did not stem from a violation of the CFL criterion in the constitutive equation. Keeping the velocity fixed and prescribed by the exact steady-state analytical expression in the constitutive equation, which was solved for the viscoelastic stress, the CFL condition leads to a much higher limit on the Weissenberg number for the same time and space discretization. Prescribing the exact solution of the viscoelastic stress in the momentum equation also leads to stable and fast convergence towards the steady-state solution for the velocity. The observations of instabilities reported in this section are valid for any time step satisfying the CFL conditions.

We have also checked that the condition of zero total flow rate is very accurately satisfied (to machine accuracy) for all computations except when the solution starts to diverge strongly. This may be a cause of long-term instabilities even if the flow rate is of the order of 10^{-6}. Enforcing this condition can be achieved by modifying accordingly the velocity at some boundary location like, for instance, at the channel exit if natural boundary conditions are used. If Dirichlet conditions for the velocity are used, the condition of zero total flow rate is always met.

Stability criterion. Using finite elements or finite differences, several authors have put forward the strong dependence of the growth rate of the perturbations on the aspect ratio of the elements rather than on the sizes of the elements themselves for the planar Couette flow problem. Keiller investigated the artificial numerical instabilities occuring in time-dependent simulation of planar Couette flow for the upper-convected Maxwell, Oldroyd-B and FENE equations [27]. Using a finite difference discretization for a creeping flow ($Re = 0$), he found that poor resolution of the continuous spectrum of eigenfunctions may lead to an instability criterion

$$We_{\text{crit}} = \mathrm{O}\left(\frac{\Delta x}{\Delta y}\right), \tag{56}$$

where Δx and Δy are, respectively, the resolution scales of the computational grid in the streamwise and cross-stream directions. Therefore it turned out that the limiting Weissenberg number was determined not by the absolute refinement of the grid but the relative refinement in the cross-stream and streamwise directions. The instability could only be removed by additional grid refinement in the cross-stream direction.

A similar scaling was established by Brown et al. [8,43] for the same problem in the context of the finite-element formulation when streamline upwind Petrov–Galerkin (SUPG) and discontinuous Galerkin (DG) methods were used to solve the hyperbolic constitutive equation of UCM and Oldroyd-B fluids.

In our simulations with the Poiseuille flow of an Oldroyd-B fluid, we found that no instability criterion as the one proposed in Eq. (56) holds in agreement with the observations of Van Kemenade and Deville [48] when they also used spectral elements for solving the corrugated planar channel problem with a steady solver. As an illustration, Fig. 9 shows the temporal evolution of the relative error of the velocity for two mesh discretizations based on the domain decomposition G1 with different polynomial orders ($N_x = 4$, $N_y = 5$) and ($N_x = 6$, $N_y = 7$) selected so that the ratio of the spacing in the two directions remains roughly constant. It can be noted in particular that the computation corresponding to the first and second discretizations are, respectively, stable and unstable for $We = 2.0$. In agreement with observations of other authors, the critical value of *We* above which oscillations appear in the solution is slightly improved when the mesh is refined in the cross-stream direction, e.g., when the polynomial order N_y is increased. On the other hand, increasing the polynomial order in the stream direction has a deleterious effect on the stability.

Influence of initial conditions. In other words, stability was found to depend strongly and mainly on Δx_{min}, the minimal mesh spacing in the streamwise direction. No substantial improvement of stability with polynomial degree or element refinement in the cross-stream direction was observed as it can be seen in the data of Table 1, which renders very complex the design of a suitable mesh at high values of *We*. Typical results are summarized in Table 1 for the Poiseuille flow of an Oldroyd-B fluid where the last column corresponds to the relative error of the velocity with respect to the analytical solution after some arbitrary number of time steps (3000) for a given time step ($\Delta t = 0.01$). The infinity symbol indicates that the run was unstable. Elements with equal size were selected for this series of runs (cf. G1 configuration in Fig. 6). From the results displayed in this table, it can be inferred that the limit value on the Weissenberg is proportional to the minimal mesh spacing in the streamwise direction.

Sources of instabilities. Instabilities might be enhanced by the use of a staggered grid for the pressure discretization. There is evidence for Newtonian flows at high Reynolds numbers that a spectral staggered grid can lead to unstable results whereas a pressure grid based on Gauss–Lobatto–Legendre inner points leads to stable ones for the same problem. Although using an inner grid for pressure improved the stability in our simulations (the maximum Weissenberg number could typically be increased by 20%), our opinion is that there is a deeper source for instabilities occuring in time-dependent problems since similar observations have been reported with different methods, e.g., in the finite difference [27] and finite element [8,43] contexts.

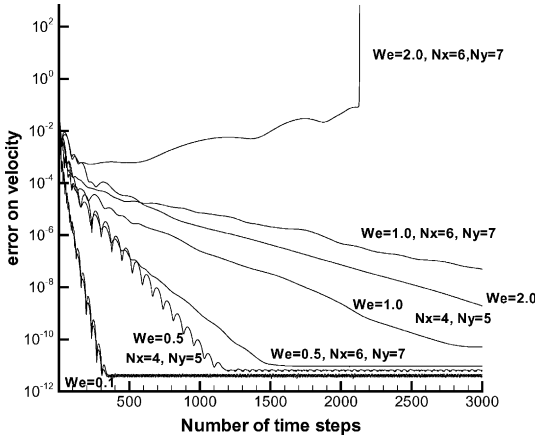

Fig. 9. Influence of the polynomial refinement (G1 configuration) on the stability and accuracy of the temporal evolution of the relative error of the velocity $\|v - v_{\text{analytical}}\|_E / \|v_{\text{analytical}}\|_E$ (Euclidean norm) (For $We = 0.1$, both curves are nearly superimposed).

Table 1
Weissenberg limiting values when the element decomposition of the domain is fixed (G1) and the polynomial orders are varied ($\Delta t = 0.01, \int_0^{H=1} v_x(y')\,dy' = 1$)

Run #	L	(NE_x, NE_y)	(N_x, N_y)	We	$\|v - v_{\text{analytical}}\|/\|v_{\text{analytical}}\|$
1	4	(2,2)	(4,5)	0.7	4.044e − 11
2	4	(2,2)	(4,5)	0.8	∞
3	8	(2,2)	(4,5)	1.3	1.624e − 06
4	8	(2,2)	(4,5)	1.4	∞
5	8	(2,4)	(4,5)	1.3	1.969e − 08
6	8	(2,4)	(4,5)	1.4	∞
7	8	(4,2)	(4,5)	0.7	1.184e − 11
8	8	(4,2)	(4,5)	0.8	∞
9	8	(2,2)	(4,7)	1.3	3.792e − 08
10	8	(2,2)	(4,7)	1.4	∞
11	8	(2,2)	(4,10)	1.3	1.027e − 08
12	8	(2,2)	(4,10)	1.4	∞
13	8	(2,2)	(4,15)	1.3	2.747e − 08
14	8	(2,2)	(4,15)	1.4	∞
15	16	(2,2)	(4,5)	2.5	3.862e − 05
16	16	(2,2)	(4,5)	2.6	3.050e − 02
17	16	(2,2)	(4,5)	2.7	∞
18	16	(4,2)	(4,5)	1.3	1.129e − 06
19	16	(4,2)	(4,5)	1.4	∞
20	32	(2,2)	(4,5)	5.0	4.591e − 03
21	32	(2,2)	(4,5)	5.2	2.332e − 01
22	32	(2,2)	(4,5)	5.4	∞
23	32	(8,2)	(4,5)	1.3	7.019e − 07
24	32	(8,2)	(4,5)	1.4	∞

The first source of instabilities is clearly the spatial discretization. In particular, one may observe wiggles developing at the element interfaces in relation to this type of instability even when solving steady equations. Numerous techniques for stabilizing finite and spectral element methods to treat steady equations for viscoelastic flows have been proposed such as the streamline upwind Petrov–Galerkin (SUPG) [10] and discontinuous Galerkin (DG) [52] methods applied to the constitutive equations, the Galerkin least square (GLS) [18] and discrete elastic viscous stress splitting (DEVSS) [25]) methods applied to the momentum equation.

The second source of instabilities definitely comes from the introduction of time in the unsteady equations. Stabilization methods adequate for the steady equations may not be as efficient for the unsteady equations, which calls for special techniques for time dependent problems. Moreover, accumulated splitting errors may result in instabilities if a decoupled approach is used.

As pointed out by Brown et al. [8] in their study of the planar Couette flow of an UCM fluid with a finite element method, accurate and numerically stable results are obtained for smooth steady-state flows while limitations due to numerical instabilities are encountered for time-dependent calculations. They identified the most dangerous modes with a real part close to $-1/2We$ and an imaginary part scaling as the streamwise wave number for moderate and large values of We in agreement with the theoretical predictions of Renardy and Renardy [40]. They asserted that these instabilities were related to the very difficult problem of calculating accurately all the contributions of the eigenspectrum to the numerical solution of the problem even for simple shear flows. Numerical boundary layer structures develop in the cross-stream direction. Similar observations can be made for the Poiseuille flow as we investigated it with a linear stability analysis. The spectrum of Poiseuille flow of UCM and Olroyd-B fluid can be determined accurately as shown by Wilson et al. [51]. Brown et al. [8] used a fully implicit integration technique to relate numerical instabilities to the

spatial discretization. They resorted to stabilization techniques including upwind techniques like SUPG to remove these instabilities up to much higher values of *We*.

In order to make a clear distinction between the two sources of instabilities, we have considered the simple Poiseuille flow benchmark problem discretized with a single element. We have then used direct solvers for treating implicitly the whole set of equations as described in Section 4.2. When using a steady-state solver, we found no limit on the Weissenberg number when the channel length has been reduced as opposed to what happens when a time-dependent algorithm is selected. On the other hand, limits on the Weissenberg number have also been found when a fully implicit unsteady solver was used to obtain the steady flows after a certain number of time steps in agreement with what is reported at the beginning of this section with our decoupled time integration technique. We have also checked that information was transmitted correctly from one element to the following when several elements are used in the mesh. One way to improve the transfer of information is to use an element-by-element solver technique already reported for steady-state computations of viscoelastic flows [11]. The solution is computed following streamlines element after element using the information coming from upstream elements to impose inflow boundary conditions on a given element. We have not found substantial improvements by applying this technique when a time-dependent algorithm is used.

Possible cures. In order to reduce the wiggles developing in the flow when the Weissenberg number was increased, we have first considered a filtering technique as proposed by Mullen and Fischer [33] for the simulation of Newtonian flows at high Reynolds numbers with spectral elements and described in Section 3.2. Typical effects of filtering the velocity and viscoelastic stress fields are shown in Fig. 10 for the domain decomposition G1 with $N_x = 4$ (streamwise direction) and $N_y = 5$ (cross-stream direction), $\alpha = 1$ and $Q_x = Q_y = 3$. Curves obtained with and without filtering and relative to two Weissenberg numbers, $We = 5.0$ and $We = 10.0$, are shown for the same geometry and mesh configuration. Clearly, filtering helps in stabilizing the computations and removes the wiggles. Various tests have been carried out with different filtering options. Either the filtering coefficient α (see Eq. (18)) or the relative orders of the filtering and original grids were allowed to vary. Optimal values of $We_{\lim}$ were always found when α was equal to 1. For each configuration characterized by the channel length and polynomial orders N_x and N_y, there seems to exist an optimal relative order of the grids. In most cases, filtering on a grid with $Q_x = Q_y = 2$ or 3 was found optimal. For best efficiency, both velocity and viscoelastic stress should be filtered.

In a second step, the stability of our computations was greatly enhanced when the DEVSS method as presented in Section 3.3 was used in combination with the filtering technique as it can be seen in Fig. 11

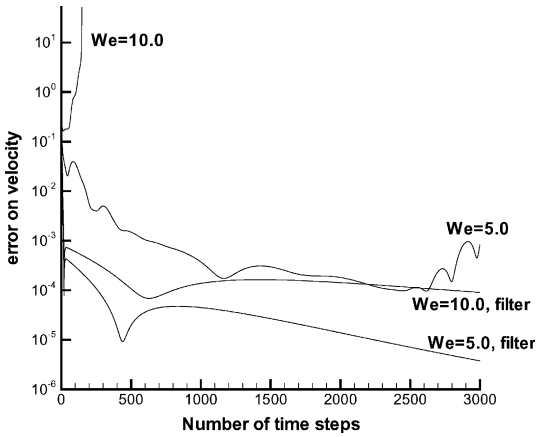

Fig. 10. Effects of filtering on the temporal variation of the relative error of the velocity $\|v - v_{\text{analytical}}\|_E / \|v_{\text{analytical}}\|_E$ (Euclidean norm) (G1 configuration, $L = 64$).

where plots of the temporal evolution of the relative error of the velocity are shown for various values of R'_μ (cf. Eq. (21)) and *We*. Tuning the additional viscosity parameter R'_μ enables to improve both stability and accuracy. When the mesh spacing in the streamwise direction is reduced, selecting very high values of R'_μ is mandatory in order to obtain stable simulations at large *We* and convergence towards the steady-state solution. As opposed to finite-element methods [8], we found no improvement by projecting the rate-of-deformation tensor or the velocity gradient on a special set of test functions when using spectral elements.

In a recent paper, Bogaerds et al. [6] have presented a comparative study of a few techniques used to stabilize finite element methods. They have selected the creeping plane Couette flow of a Maxwell fluid as a benchmark to determine the temporal stability of numerical algorithms. They emphasized the unstable behavior of the DG method, which allow for discontinuous approximations of the viscoelastic stress when time-dependent algorithms are used. Stable results up to very high Weissenberg numbers were obtained when the DEVSS formulation was used in conjunction with the SUPG method.

We have tried to improve the stabilitity of the Poiseuille flow of an Oldroyd-B fluid simulated with our time-dependent algorithm by using the SUPG method but without substantial improvement.

6.3.2. FENE models with finite extensibility

So far, results obtained with the Oldroyd-B or UCM models corresponding to a FENE model with infinite extensibility using various techniques (Galerkin, filtering, DEVSS) have shown that it is very difficult to obtain stability for the simple planar Poiseuille flow at large Weissenberg number without stabilization or that stability for steady flows is achieved at the expense of introducing additional artificial viscosity, which can be detrimental to a correct description of the physics involved in a transient flow as underlined by Smith et al. [43].

It is well known that there are many other models that are more stable than the Oldroyd-B one. All the following results are relative to geometry G2 with a total channel length $L = 64$ (cf. Fig. 6), a Galerkin discretization (i.e. without stabilization technique) so that they can be compared to the results for the Oldroyd-B fluid visible in Fig. 8.

Stable results have been obtained when using models of the FENE family as shown in Fig. 12 for the FENE-P and FENE-CR models for a relatively small (arbitrary) value of the extensibility parameter L_e equal to $\sqrt{6}$. For this value of L_e, results of the simulations were found stable and independent on the channel mesh L, at least for $4 \leqslant L \leqslant 64$. When L_e tends to infinity, one gets back the Oldroyd-B model. The

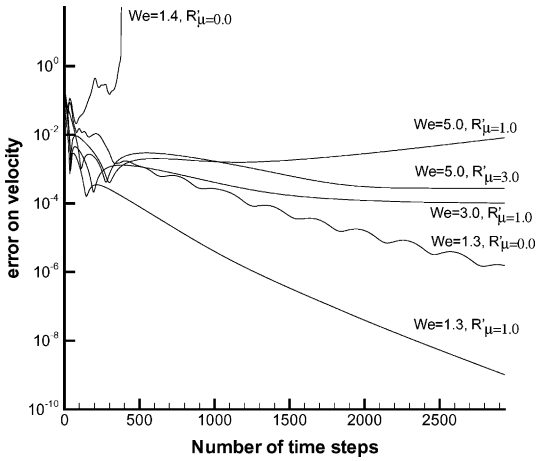

Fig. 11. Influence of the DEVSS parameter on the stability of the temporal evolution of the relative error of the velocity $\|v - v_{\text{analytical}}\|_E / \|v_{\text{analytical}}\|_E$ (Euclidean norm) (G1 configuration, $L = 16$).

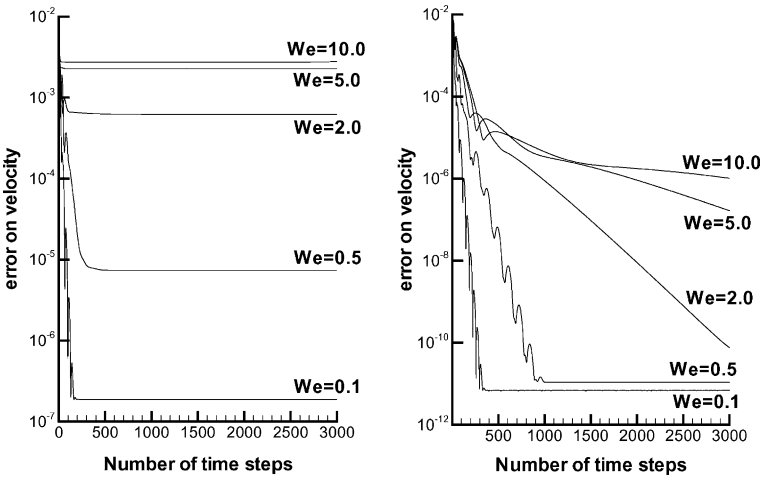

Fig. 12. Temporal evolution of the relative error of the velocity $\|v - v_{\text{analytical}}\|_E / \|v_{\text{analytical}}\|_E$ (Euclidean norm) (G2 configuration, $L = 64$) for the planar Poiseuille flows of FENE-P (left) and FENE-CR (right) ($L_e = 6$, $K = 1 - (3/L_e^2)$).

Weissenberg limit occuring in the simulations for a fixed mesh has been found dependent on L_e. At a given value of *We*, the normal stress component τ_{xx} is an increasing function of L_e so that the Oldroyd-B model leads to a much higher level of stress in the streamwise direction that the FENE-CR model with a low value of L_e (keeping the other parameters identical).

The upper-convected derivative term is multiplied by a moderating factor $(1 - (\text{tr}(\mathbf{A})/L_e^2))$ in models of the FENE-type (cf. Eq. (6) as opposed to the vast majority of other models) which result in adding more terms in the constitutive equation while keeping the same factor (equal to 1) for the upper-convected derivative as in the Oldroyd-B model. As the Weissenberg number increases, the infinite norm of this factor decreases, which helps in reducing potential instabilities induced by the upper-convected derivative operator in the constitutive equation.

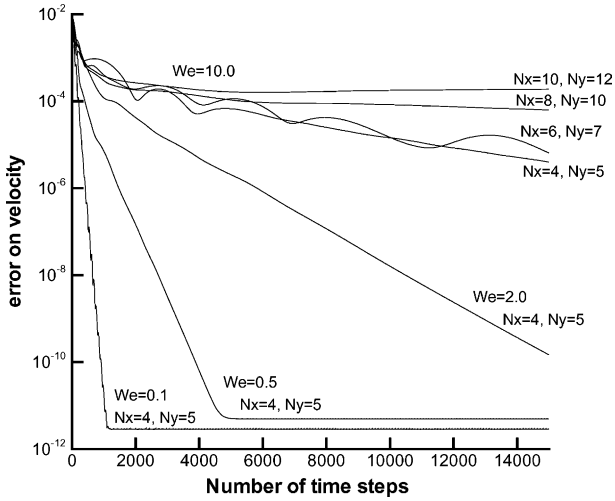

Fig. 13. Temporal evolution of the relative error of the velocity $\|v - v_{\text{analytical}}\|_E / \|v_{\text{analytical}}\|_E$ (Euclidean norm) (G1 configuration, $L = 4$) for the planar Poiseuille flow of a FENE-CR fluid ($L_e = 6$, time step: $\Delta t = 0.002$).

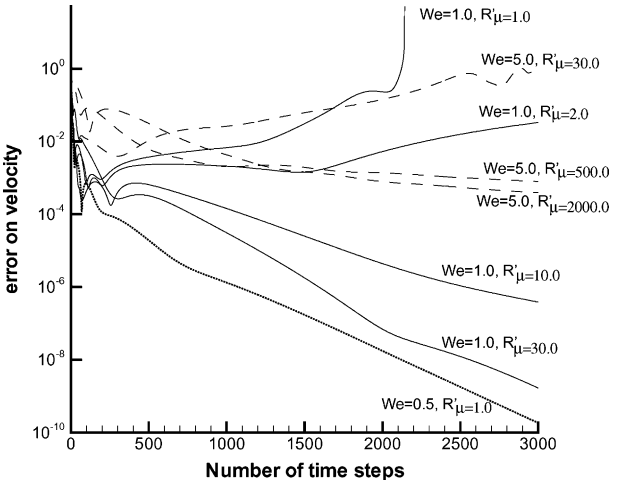

Fig. 14. Temporal evolution of the relative error of the velocity $\|v - v_{\text{analytical}}\|_E / \|v_{\text{analytical}}\|_E$ (Euclidean norm) (G1 configuration, $L = 4$, $N_x = 4$, $N_y = 5$) for the planar Poiseuille flow of an Oldroyd-B with the DEVSS formulation and filtering.

The same type of plot is given for the FENE-CR model (Fig. 13) for $L_e = 6$ when the channel length is reduced from 64 to 4 while keeping the same number of elements and polynomial orders (geometry G1 in Fig. 6). For the sake of comparison, the computation for the Oldroyd-B model with the same geometry and discretization is unstable at $We = 0.6$ for $N_x = 4$ and $N_y = 5$. It is visible in Fig. 13 that the stability of the simulation is much less sensitive to the mesh discretization with the FENE-CR model (at least for low values of L_e).

Fig. 14 shows what values of the stabilization parameter R'_μ of the DEVSS method with filtering must be selected in order to be able to reach similar Weissenberg numbers for the corresponding Oldroyd-B fluid in the same configuration. Even for moderate values ($We \simeq 5.0$) of the Weissenberg number, very high values of the additional artificial viscosity ($R'_\mu \simeq 500$) must be introduced to get stable and accurate results for the simple steady flows if the size of the computational domain in the streamwise direction is small. It is doubtful that using such a technique for a truly time-dependent problem (i.e., where transient phenomena should be accurately observed) would be adequate as indicated in Section 6.1.

7. Conclusions

We have presented a method based on the spectral element formulation for the simulation of time-dependent flows of viscoelastic fluids for various types of constitutive equations. It has been tested on simple steady and unsteady Poiseuille flows as well as a more complex flow in an abrupt contraction. As opposed to simulations of Poiseuille flows with models of the FENE type with low values of the extensibility parameter L_e, which have been found stable for various discretizations, the stability of the results obtained with the Oldroyd-B model has been shown to be strongly dependent on the computational grid. Then, it could be only improved by using a special filtering technique combined with the DEVSS method.

There is a growing interest in developing numerical tools to investigate the onset of instabilities observed in experiments involving viscoelastic flows [28]. Our goal is to use the spectral element method to resolve such physical instabilities like, e.g., the ones occuring in contractions as the Weissenberg number is increased [31]. Numerical methods are prone to artificial instabilities which can be removed by so-called stabilization techniques, which are generally well suited for steady problems. One major drawback is that

these techniques may introduce unsuitable effects in the simulations that may also prevent physical instabilities to develop [43]. The present studies for the Poiseuille and abrupt contraction suggest that simulations of complex benchmark problems should preferably be carried out using the FENE models (FENE-CR for fluids with constant shear viscosity and FENE-P for shear-thinning fluids) with low values of the extensibility parameter without additional stabilization techniques. Special tools like the ones described in [43] will be needed to diagnose the type of instabilities (numerical or physical) when they appear in complex flows by determining accurately the most unstable modes.

Acknowledgements

This research was partially funded by a Swiss National Science Foundation Grant (No. 20-59357.99), whose support is gratefully acknowledged.

References

[1] C. Bernardi, N. Fiétier, R.G. Owens, An error indicator for mortar element solutions to the Stoke's problem, IMA J. Num. Anal. 21 (2001) 857–886.
[2] C. Bernardi, Y. Maday, A.T. Patera, A new nonconforming approach to domain decomposition: the mortar element method, in: H. Brezis, J.-L. Lions (Eds.), Nonlinear Partial Differential Equations and Their Applications, Collège de France seminar XI, Pitman, 1994, pp. 13–51.
[3] F. Ben Belgacem, C. Bernardi, N. Chorfi, Y. Maday, Inf-sup conditions for the mortar element discretization of the Stoke's problem, Numer. Math. 85 (2000) 257–281.
[4] R.B. Bird, J.R. Deaguiar, An encapsulated dumbbell model for concentrated polymer solutions and melts. I. theoretical development and constitutive equation, J. Non-Newtonian Fluid Mech. 13 (1983) 149–160.
[5] C. Bodart, M.J. Crochet, Time-dependent numerical simulation of viscoelastic flow and stability, Theoret. Comput. Fluid Dyn. 5 (1993) 57–75.
[6] A. Bogaerds, G. Peters, F. Baaijens, Temporal stability of low-order continuous and discontinuous mixed finite element techniques for viscoelastic fluid mechanics, in: Proceedings of the XIIIth International Congress on Rheology, Cambridge, UK, 2000, pp. 2199–2201.
[7] J. Bonvin, M. Picasso, Variance reduction methods for CONNFFESSIT-like simulations, J. Non-Newtonian Fluid Mech. 84 (1999) 191–215.
[8] R.A. Brown, M.J. Szady, P.J. Northey, R.C. Armstrong, On the numerical stability of mixed finite-element methods for viscoelastic flows governed by differential constitutive equations, Theoret. Comput. Fluid Dyn. 5 (1993) 77–106.
[9] C. Canuto, M.Y. Hussaini, A. Quarteroni, T.A. Zang, Spectral Methods in Fluid Dynamics, Springer, New York, 1988.
[10] C. Chauvière, R.G. Owens, How accurate is your solution? Error indicators for viscoelastic flow calculations, J. Non-Newtonian Fluid Mech. 95 (2000) 1–33.
[11] C. Chauvière, R.G. Owens, A new spectral element method for the reliable computation of viscoelastic flow, Comput. Meth. Appl. Mech. Eng. 190 (2001) 3999–4018.
[12] M.D. Chilcott, J.M. Rallison, Creeping flow of dilute polymer solutions past cylinders and spheres, J. Non-Newtonian Fluid Mech. 29 (1988) 381–432.
[13] W. Couzy, M. Deville, Spectral element preconditioners for the Uzawa pressure operator applied to incompressible flows, J. Sci. Comput. 9 (1994) 107–122.
[14] W. Couzy, Spectral element discretization of the unsteady Navier–Stokes equations and its iterative solution on parallel computers, Ph.D thesis No. 1380, Department of Mechanical Engineering, Ecole Polytechnique Fédérale de Lausanne, 1995.
[15] W. Couzy, Iterative solutions of the 3D transient Navier–Stokes equations on parallel computers, in: A.V. Ilin, L.R. Scott (Eds.), Houston J. Math., 1996, pp. 585–593.
[16] M.O. Deville, P.F. Fischer, E.H. Mund, High-order Methods for Incompressible Fluid Flow, Cambridge University Press, New York, 2002.
[17] Y. Dubois-Pèlerin, V. Van Kemenade, M.O. Deville, An object-oriented toolbox for spectral element analysis, J. Sci. Comput. 14 (1999) 1–29.
[18] Y. Fan, R.I. Tanner, N. Phan-Thien, Galerkin/least-square finite-element methods for steady viscoelastic flows, J. Non-Newtonian Fluid Mech. 84 (1999) 233–256.

[19] N. Fiétier, M.O. Deville, Spectral element methods for unsteady viscoelastic flows, in: Proceedings of the 16th IMACS World Congress, Swiss Federal Institute of Technology-Lausanne, Switzerland, 2000, 129.3B.
[20] N. Fiétier, M.O. Deville, Simulations of time-dependent flows of viscoelastic fluids with spectral element methods, J. Sci. Comput. 17 (2002) 699–707.
[21] N. Fiétier, Numerical simulations of viscoelastic fluid flows of spectral element methods and time-dependent algorithms, Ph.D. thesis No. 2631, Department of Mechanical Engineering, Ecole Polytechnique Fédérale de Lausanne, 2002.
[22] N. Fiétier, M.O. Deville, Linear stability analysis of time-dependent algorithms with spectral element methods for the simulation of viscoelastic flows, J. Non-Newtonian Fluid Mech., accepted for publication.
[23] M.I. Gerritsma, T.N. Phillips, Discontinuous spectral element approximations for the velocity–pressure–stress formulation of the Stokes problem, Int. J. Numer. Meth. Eng. 43 (1998) 1401–1419.
[24] M.I. Gerritsma, T.N. Phillips, Compatible spectral approximations for the velocity–pressure–stress formulation of the Stokes problem, SIAM J. Sci. Comput. 20 (1999) 1530–1550.
[25] R. Guénette, M. Fortin, A new mixed finite element method for computing viscoelastic flows, J. Non-Newtonian Fluid Mech. 60 (1995) 27–52.
[26] G. Em Karniadakis, M. Israeli, S.A. Orszag, High-order splitting methods for the incompressible Navier–Stokes equations, J. Comput. Phys. 97 (1991) 414–443.
[27] R.A. Keiller, Numerical instability of time-dependent flows, J. Non-Newtonian Fluid Mech. 43 (1992) 229–246.
[28] R.G. Larson, Instabilities in viscoelastic flows, Rheol. Acta 31 (1992) 213–263.
[29] Y. Maday, A.T. Patera, Spectral element methods for the incompressible Navier–Stokes equations, in: A.K. Noor, J.T. Oden (Eds.), State-Of-The-Art Surveys on Computational Mechanics, The American Society of Mechanical Engineers, New York, 1989, pp. 71–143.
[30] Y. Maday, A.T. Patera, E.M. Rønquist, An operator-integration-factor splitting method for time-dependent problems: application to incompressible fluid flow, J. Sci. Comput. 5 (1990) 263–292.
[31] G.H. McKinley, W.P. Raiford, R.A. Brown, R.C. Armstrong, Nonlinear dynamics of viscoelastic flow in axisymmetric abrupt contractions, J. Fluid Mech. 223 (1991) 411–456.
[32] T.C.B. McLeish, R.G. Larson, Molecular constitutive equations for a class of branched polymers: The Pom-Pom polymer, J. Rheol. 42 (1998) 81–110.
[33] J.S. Mullen, P.F. Fischer, Filtering techniques for complex geometry fluid flows, Comm. Numer. Meth. Eng. 15 (1999) 9–18.
[34] P.J. Northey, R.C. Armstrong, R.A. Brown, Finite element calculation of time-dependent two-dimensional flow with the explicitly elliptic momentum equation formulation, J. Non-Newtonian Fluid Mech. 36 (1990) 117–139.
[35] R.G. Owens, T.N. Phillips, Decoupled spectral element methods for steady viscoelastic flow past a sphere, in: A.V. Ilin, L.R. Scott (Eds.), Proceedings of the Third International Conference on Spectral and High Order Methods, Houston Journal of Mathematics, Houston, USA, 1996, pp. 287–294.
[36] T.C. Papanastasiou, N. Malamataris, K. Ellwood, A new outflow boundary condition, Int. J. Numer. Meth. Fluids 14 (1992) 587–608.
[37] J. Blair Perot, An analysis of the fractional step method, J. Comput. Phys. 108 (1993) 51–58.
[38] N. Phan-Thien, A nonlinear network viscoelastic model, J. Rheol. 22 (1978) 259–283.
[39] B. Purnode, M.J. Crochet, Flows of polymer solutions through contractions. Part1: flows of polyacrylamide solutions through planar contractions, J. Non-Newtonian Fluid Mech. 65 (1996) 269–289.
[40] M. Renardy, Y. Renardy, Linear stability of plane Couette flow of an upper convected Maxwell fluid, J. Non-Newtonian Fluid Mech. 22 (1986) 23–33.
[41] E.M. Rønquist, Spectral element methods for the unsteady Navier–Stokes equations, Lecture Series 1991-01, von Karman Institute for Fluid Dynamics, Belgium, 1991.
[42] Y. Saad, M. Schulz, GMRES: A generalized minimal residual algorithm for solving nonsymmetric linear systems, SIAM J. Sci. Statist. Comput. 7 (1986) 856–869.
[43] M.D. Smith, R.C. Armstrong, R.A. Brown, R. Sureshkumar, Finite element analysis of stability of two-dimensional viscoelastic flows to three-dimensional perturbations, J. Non-Newtonian Fluid Mech. 93 (2000) 203–244.
[44] M. Somasi, B. Khomami, Linear stability and dynamics of viscoelastic flows using time-dependent stochastic simulation techniques, J. Non-Newtonian Fluid Mech. 93 (2000) 339–362.
[45] R. Sureshkumar, A.N. Beris, Linear stability of viscoelastic Poiseuille flow using an Arnoldi-based orthogonalization algorithm, J. Non-Newtonian Fluid Mech. 56 (1995) 151–182.
[46] R. Sureshkumar, M.D. Smith, R.C. Armstrong, R.A. Brown, Linear stability and dynamics of viscoelastic flows using time-dependent numerical simulations, J. Non-Newtonian Fluid Mech. 82 (1999) 57–104.
[47] L.J.P. Timmermans, P.D. Minev, F.N. Van de Vosse, An approximate projection scheme for incompressible flow using spectral elements, Int. J. Numer. Meth. Fluids 22 (1996) 673–688.
[48] V. Van Kemenade, M.O. Deville, Application of spectral elements to viscoelastic creeping flows, J. Non-Newtonian Fluid Mech. 51 (1994) 277–308.

[49] N.D. Waters, M.J. King, Unsteady flow of an elastico-viscous liquid, Rheol. Acta 9 (1970) 345–355.
[50] D. Weill, M.O. Deville, Steady gap flows by the spectral and mortar element method, J. Sci. Comput. 17 (2002) 639–648.
[51] H.J. Wilson, M. Renardy, Y. Renardy, Structure of the spectrum in zero Reynolds number shear flow of the UCM and Oldroyd-B liquids, J. Non-Newtonian Fluid Mech. 80 (1999) 251–268.
[52] F. Yurun, A comparative study of the discontinuous Galerkin and continuous SUPG finite element methods for computation of viscoelastic flows, Comput. Meth. Appl. Mech. Eng. 141 (1997) 47–65.